

Proc. of the 17th Int. Conference on Digital Audio Effects (DAFx-14), Erlangen, Germany, September 1-5, 2014

EXAMINING THE OSCILLATOR WAVEFORM ANIMATION EFFECT

Joseph Timoney¹ and Victor Lazzarini¹,

¹Sound and Music Technology research group,
NUI Maynooth
Maynooth, Ireland
joseph.timoney@nuim.ie
victor.lazzarini@nuim.ie

Jari Kleimola², and Vesa Välimäki³,

²Dept. of Media Technology
³Dept. of Signal Processing and Acoustics
Aalto University, Espoo, Finland
jari.kleimola@aalto.fi
vesa.valimaki@aalto.fi

ABSTRACT

An enhancing effect that can be applied to analogue oscillators in subtractive synthesizers is termed Animation, which is an efficient way to create a sound of many closely detuned oscillators playing in unison. This is often referred to as a supersaw oscillator. This paper first explains the operating principle of this effect using a combination of additive and frequency modulation synthesis. The Fourier series will be derived and results will be presented to demonstrate its accuracy. This will then provide new insights into how other more general waveform animation processors can be designed.

1. INTRODUCTION

The modelling of analogue musical equipment using digital techniques has been an area of research that has received considerable attention over the past decade, and is still a very current topic [1]. This field covers the reproduction of Tube amplifiers ([2] and [3]), guitar effects devices ([4] and [5]), spring reverb units [6], analog synthesizer oscillators, both generally in [7] and [8], and in a model specific manner in [9] and [10], and resonant voltage controlled filters ([11], [12], and [13]).

With regard to analog synthesizer oscillators in particular, most of the previous work has focused on the alias-free synthesis of ideal classical waveforms, such as the sawtooth, the triangle, and the rectangular waveforms, see [7], or [14], for example. The reason for this focus on oscillators was simply that digital models of waveforms associated with particular analog synthesizers are more difficult to create because it requires access to such synthesizers in order to make waveform measurements. These can be expensive and difficult to obtain in their vintage versions. The ideal forms of the classic waveform signals have a spectrum that decays about 6 or 12 dB per octave, following the $1/f$ or the $1/f^2$ law (where f denotes frequency), respectively [19].

An early approach was the filtering of the digital impulse train obtained from the summation formula for the cosine series [20]. More recent works have proposed to implement an approximately bandlimited impulse train using a windowed sinc table ([21] and [22]), a feedback delay loop including an allpass filter [24], or a sequence of impulse responses of fractional delay filters [25]. Alternative approaches include the differentiated polynomial waveforms ([26],[27] and [28]), hyperbolic waveshaping [8], Modified FM synthesis[29], polynomial interpolation [30], polynomial transition regions [15] and [18], bandlimited impulse train generation using analog filters [16], and nonlinear phase basis functions [17].

Alongside these oscillator algorithms, other work has focused on enhancing effects that can be applied to them such as

Hard Synchronisation ([31] and [32]) and Frequency Modulation ([33] and [34]).

One very interesting effect is described in the literature as Waveform Animation [35]. Animation is a single oscillator effect. It is an enhancement to the traditional non-modular analogue subtractive synthesizers feature of two or three oscillators per voice ([36] and [37]), which has generally held up for digital emulations [38]. The result of the Animation is the production of a deep, thick, pulsing sound. Originally proposed as a technique for modular analog systems it did not appear on synthesizers produced by the major manufacturers who opted for simply adding a unison oscillator option instead ([39] and [40]). More recently this unison oscillator arrangement has become termed as a *Supersaw* [38] or a *Hypersaw* [41]. It became strongly associated with electronic dance music.

Nam *et al.* [25] proposed an implementation of this effect in which several detuned bandlimited impulse trains (BLITs) with appropriate DC offsets are added together and fed through a single leaky integrator. However, this incurs the computational costs of generating multiple waveforms at a small frequency difference from each other. A digital implementation of Waveform animation, however, offers a more efficient alternative for creating this multiple oscillator sound effect than just adding numerous detuned waveforms because it does not result in a corresponding loss in polyphony as groups of oscillators are assigned to each voice.

When it comes to the digital emulation of a particular analog effect there are two choices: either (1) attempt to reproduce a particular analog circuit design directly or (2) to emulate the operation from an algorithmic perspective with tailored digital elements. While the first approach can work very well, it produces an algorithm that is computationally intensive and requires a significant oversampling factor to operate correctly, see [5], [11], [12], and [13]. The second approach is less complex, computationally cheaper, and more flexible, conferring the final implementation with benefits such as having greater polyphony available to the virtual synthesizer. An example of this approach has been presented in [10].

Therefore, in this paper, we will work out the underlying theory of the Waveform Animator oscillator effect from a signals point of view. This will be augmented by a model by which it can be implemented efficiently in modern digital synthesis systems using delay lines. The next section will mention the origins of the effect combined with the theory underlying it.

2. MULTIPLE DETUNED OSCILLATORS

The idea for this sound can be attributed to Risset [42] who de-

veloped it in the late 1960s for some of his compositions. In computer music circles it is sometimes termed the ‘Risset Arpeggio’ [43]. The intense effect of the detuned sound is due to a complicated beating pattern created among the harmonics of each oscillator. An analytical expression is available that describes this pattern [44]. Assuming a signal with a number of harmonics that has M detuned copies at a spacing of δf_0 between each of them, the beating pattern amplitude of the k^{th} complex harmonic cluster is given by

$$B_k(t) = A_k \frac{\sin(\pi M k \delta f_0 t)}{\sin(\pi k \delta f_0 t)} \quad (1)$$

where A_k is the amplitude of the k^{th} harmonic.

3. WAVEFORM ANIMATOR

Hutchins proposed the multiphase waveform animator capable of emulating a bank of detuned sawtooth oscillators with a single Voltage Control Oscillator (VCO), by mixing a number of algebraically phase shifted sawtooth waveforms together [35]. The original paper did not show mathematically how this is achieved; rather it was demonstrated in terms of the waveforms it required as it was intended for implementation using a modular analog synthesis system. However, to gain a deeper insight that will assist our digital implementations it is worthwhile to understand the principle of this system fully.

The input to the Animator is a sawtooth with a rising edge of amplitude A . The animator itself consists of a number of channels each controlled by a different triangle wave Low Frequency Oscillator (LFO), whose rate should be less than 2Hz and whose amplitude is smaller than that of the input [35]. A block diagram of one channel that illustrates the principle of the animator is given in Fig. 1. Note that more channels leads to a more intense effect.

In Fig. 1, the input sawtooth and LFO are on the left hand side, there are two subtracting elements, a comparator, and the output appears on the right hand side. This output is a time-varying phase-shifted sawtooth that is then added with the input sawtooth to create the animated effect.

To explain in more detail: subtracting the input from the LFO generates an intermediate waveform. The LFO is very slow in relation to the input so that it is effectively like adding a DC offset to each period of the input wave. Fig. 2 shows this graphically using the relevant waveforms. In Fig. 2 the amplitude of the input sawtooth $A = 5.0$ and the amplitude of the LFO is 2.0. The result of the operation is that the DC level of the input is altered by a value of 7.0 in this example.

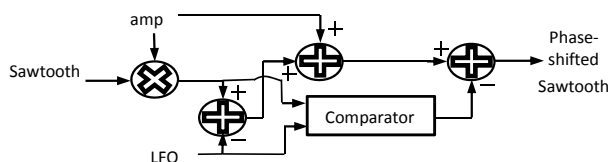


Figure 1. Block diagram of one channel of the waveform animator.

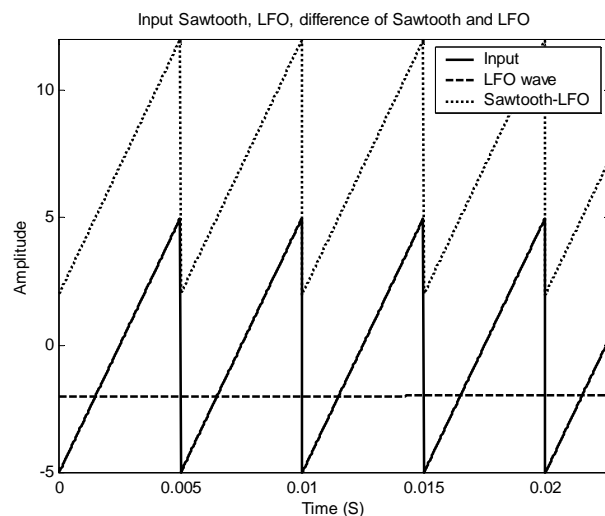


Figure 2. Input sawtooth (solid line), LFO waveform (dashed line) and difference of the two (dotted line).

This waveform is fed to a comparator device that is set to emit a pulse when its input is greater than the sawtooth amplitude A , otherwise the output is zero. This results in a PWM waveform whose pulse is on the leading edge and whose pulse width is varying at the rate of the LFO. Further, the amplitude of the pulse is $2A$. This PWM wave is then subtracted from the DC-altered sawtooth to produce a time-varying phase-shifted version of the input sawtooth. This is illustrated in Fig. 3. The upper panel shows the generated PWM wave against the comparator input and the lower panel shows the original input sawtooth and its phase shifted version.

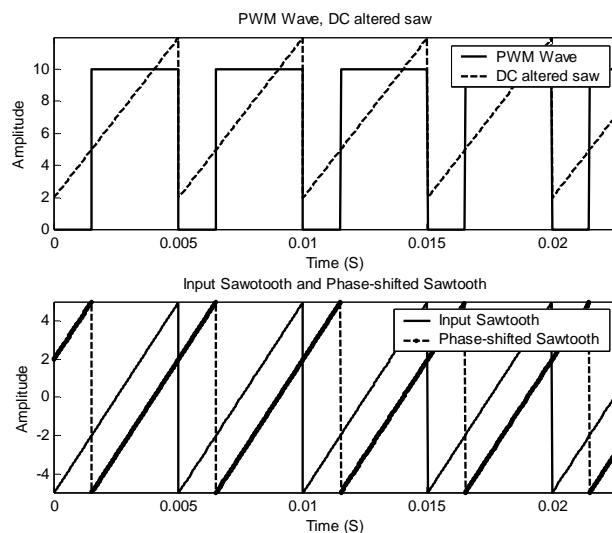


Figure 3. The DC-altered sawtooth (dashed line) and PWM wave (solid line) at the output of the comparator are given in the upper panel. The input sawtooth (solid line) and the resulting phase-shifted sawtooth (dashed line) are shown in the lower panel.

To illustrate mathematically what the animator is doing, first assume that we are looking only over a few periods where the

LFO waveform can be regarded as a constant DC level, we can then write the animator output as

$$S_{wa}(t) = -\frac{2A}{\pi} \sum_{k=1}^{\infty} \frac{\sin(2\pi k f_0 t)}{k} + C_{dc} - P_{zs}(t) \quad (2)$$

where the first term on the rhs of (2) denotes a rising sawtooth, C_{dc} represents the added DC level, and the third term represents the PWM waveform comparator output whose maximum amplitude is $2A$ and minimum value is zero.

The expression for a falling edge, zero-centered, PWM wave of time-varying duty cycle $d(t)$ is [45]

$$P(t) = d(t) + \sum_{k=1}^{\infty} \frac{\sin(2\pi k d(t) - k 2\pi f_0 t)}{(k\pi)} + \sum_{k=1}^{\infty} \frac{\sin(k 2\pi f_0 t)}{(k\pi)} \quad (3)$$

Each component of the second term on the rhs of (3) is phase shifted where the phase shift depends both on the duty cycle and increases with increasing frequency because of the factor k . To rewrite (3) so that it represents the comparator output correctly it needs to have a leading edge pulse and be scaled in amplitude

$$P_{zs}(t) = -(2A)P(t) + 2A \quad (4)$$

Substituting (3) into (4), and then the result into (2) we can write the animator output as a combination of AC and DC components.

$$S_{wa}(t) = S_{AC}(t) + S_{DC}(t) \quad (5)$$

Remembering from (2) that the comparator combines the PWM wave along with the input sawtooth if we concentrate on the AC components of (5) first we have

$$S_{AC}(t) = 2A \left(\sum_{k=1}^{\infty} \frac{\sin(2\pi k d(t) - k 2\pi f_0 t)}{(k\pi)} + \sum_{k=1}^{\infty} \frac{\sin(k 2\pi f_0 t)}{(k\pi)} \right) - 2A \sum_{k=1}^{\infty} \frac{\sin(k 2\pi f_0 t)}{k\pi} \quad (6)$$

which can be written as

$$S_{AC}(t) = -2A \sum_{k=1}^{\infty} \frac{\sin(k 2\pi f_0 t - 2\pi k d(t))}{(k\pi)} \quad (7)$$

This gives the equation for a rising sawtooth with a time-varying phase shift. Then, looking at the DC term of (5)

$$S_{DC}(t) = DC - 2A + 2Ad(t) \quad (8)$$

The term $d(t)$ will be constant within each time period. Thus, for a single time period we can write

$$S_{DC} \approx DC - 2A + 2A\hat{d} \quad (9)$$

To show that (9) is zero, we must determine \hat{d} by locating the point of intersection of the LFO waveform with the sawtooth waveform in each period. If we write these as line equations we

can use simple geometry to determine the intersection point between the two. For argument's sake, we assume that we are examining the crossing point within the first period of the sawtooth wave. Doing this, the time of their intersection t_p can be expressed as

$$t_p = \frac{A - A_{LFO}}{(2Af_0 - 2A'_{LFO}f_{LFO})} \quad (10)$$

where f_{LFO} is the LFO frequency, $A_{LFO}(t)$ is the time-varying amplitude of the LFO wave and A'_{LFO} is the maximum amplitude it will reach within that one period. The value of the duty cycle for that period will be

$$\hat{d} = \frac{(Af_0 - A'_{LFO}f_0)}{(2Af_0 - 2A'_{LFO}f_{LFO})} \quad (11)$$

To further simplify the analysis we assume that within this first period of the sawtooth the amplitude of the triangle wave is constant, i.e.

$$A'_{LFO} = A_{LFO} \quad (12)$$

Then, examining Fig. 2, we can write

$$DC \approx A + A_{LFO} \quad (13)$$

Substituting (12) into (11) and then combine with (13) in (9) to give

$$S_{DC} = A + A'_{LFO} - 2A + 2A \frac{(Af_0 - A'_{LFO}f_0)}{(2Af_0 - 2A'_{LFO}f_{LFO})} \quad (14)$$

Next, noting that

$$(2Af_0 \gg 2A'_{LFO}f_{LFO}) \quad (15)$$

The third term on the rhs of (14) can then be approximated, and following simple manipulation leads to the expected result

$$S_{DC} = A + A'_{LFO} - 2A + A - A'_{LFO} = 0 \quad (16)$$

The expression (16) will hold for every period of the input sawtooth. Therefore, the final animator output can be written

$$S_{wa}(t) = -2A \sum_{k=1}^{\infty} \frac{\sin(k 2\pi f_0 t - 2\pi k d(t))}{(k\pi)} \quad (17)$$

Examining (17) it can be interpreted as a summation of harmonically related frequency modulated sinusoids where the modulation is the time-varying duty cycle $d(t)$ and the modulation index increases with respect to the harmonic number. This result is very interesting as it means that the bandwidth around each harmonic increases with respect to increasing frequency. This would suggest why the waveform is perceived as being 'animated' as this increasing bandwidth with respect to frequency is similar in effect to adding detuned harmonic waveforms together. Furthermore, the faster the LFO the wider the bandwidth will become. There also should be a relationship between the swing in

the duty cycle with the sideband harmonic magnitudes and ultimately the strength of the effect.

4. ANIMATOR SPECTRAL PROPERTIES

It is worthwhile to investigate the spectral properties of the animated waveform a little further. The time-varying duty cycle signal only changes its value for every new period of the input sawtooth. This means that this modulating duty wave resembles a flat-top multi-level Pulse Amplitude Modulation signal, where the pulse rate is the same as the input sawtooth. However, because it is changing so slowly to simplify the analysis first we can assume that the duty cycle modulation is a shifted and scaled triangle LFO of the form

$$d(t) = \left(\frac{d_{\max} + d_{\min}}{2} \right) - \left(\frac{d_{\max} - d_{\min}}{2} \right) \text{tri}(2\pi f_{LFO} t) \quad (18)$$

where d_{\max} and d_{\min} are the maximum and minimum values of the duty cycle respectively. They are determined by the user choice for A_{LFO} .

We can also write the Fourier series for the triangle wave modulation in (18) as

$$\text{tri}(2\pi f_{LFO} t) = \sum_{k_1} \frac{8}{(q\pi)^2} \cos(2\pi q f_{LFO} t - \pi), \quad q = 1, 3, 5, \dots \quad (19)$$

where q is the harmonic index.

This particular triangle wave will start from its minimum value which is in keeping with the original work [35]. Combining (19) with (18) and then substituting into (17) we can see that we will have a Complex FM waveform [46]. The relative contribution of each harmonic of the LFO to the spectrum of (17) could be computed using this theory. However, it can quickly become complicated if we use many components from the Fourier series in (19). By writing expressions for the modulation indices it is possible to find a way of simplifying the task. Denoting the magnitudes of the modulation indices for each as I_q we can consider the first two significant components (The second harmonic magnitude $I_2=0$ because it is a triangle wave) we have

$$I_1 = \frac{8}{\pi} (d_{\max} - d_{\min}) \quad (20)$$

and

$$I_3 = \frac{8}{9\pi} (d_{\max} - d_{\min}) \quad (21)$$

Noting that $I_1 > 1$ while $I_3 \ll 1$ (and will be true for all higher modulation indices), this suggests that it would be reasonable to assume that the primary contribution to the modulation of each harmonic in (17) is only the first component with modulation index given by (20) which allows us to rewrite

$$S_{wa}(t) = -2A \sum_{k=1}^{\infty} \frac{\sin(k2\pi f_0 t + kI_1 \cos(2\pi f_{LFO} t) + \vartheta)}{(k\pi)} \quad (22)$$

where we denote the phase shift $\vartheta = -k\pi(d_{\max} + d_{\min})$.

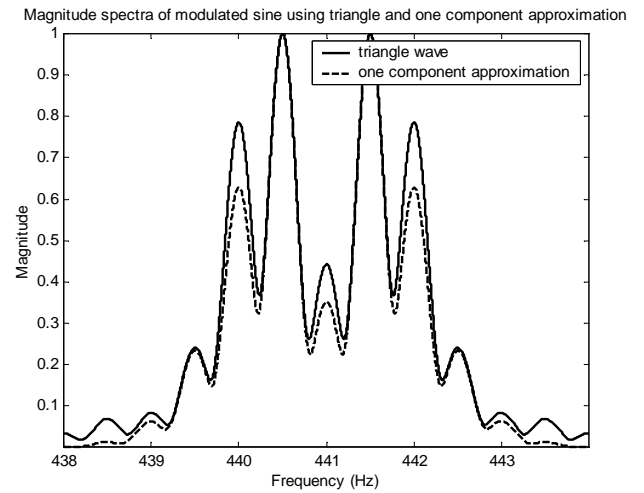


Figure 4. Comparison of the spectra of a sine wave that has been frequency modulated using the triangle wave LFO of (19) (solid line) versus a one component approximation to it as given by (22) (dashed line).

To validate the approximation Fig. 4 shows a plot of the spectra of a frequency modulated single sine wave of frequency 441Hz using the modulation function of (18) with frequency 0.5Hz and $d_{\max}=0.9$ and $d_{\min}=0.1$ (solid line) along with the spectrum of the same sine wave but with a sine wave modulation function with modulation index given by (20). From the figure it can be seen that there is an exact match for the magnitude of the first and third order sidebands at 441.5Hz, 440.5Hz, 442.5Hz and 439.5Hz respectively. There is a close match with the second order sidebands at 442Hz and 440Hz. This indicates that the approximation is acceptable.

Once adopting this approximation it is straightforward to have an expression for the magnitude spectrum of (22) around each harmonic

$$|H(kf_0 + nf_{LFO})| = (J_o(kI_1)) \quad (23)$$

where J_o denotes a Bessel function of order o [47].

With this done it is possible to plot a relationship between the width of the duty cycle (that is, the difference between the maximum and minimum values) versus the magnitude of the first sideband of the modulation. This is helpful when creating an animated waveform as it can be used to decide how to set the amplitude of the triangle wave LFO and to determine the amplitudes of other sawtooths that could be added to the animated wave to get a desired balance between the animated waves and the original. This is similar to the mix function associated with commercial products [38], [41]. An experiment can be run by creating different values for the first modulation index in (20) using different values of duty cycle width. These can then be substituted into (23) to compute the first sideband magnitude (where $o = 1$). The result of this is given in Fig. 5. It shows that the largest sideband magnitude occurs when the width of the duty cycle is 0.7. This corresponds to a duty cycle maximum of 0.85 and a duty cycle minimum of 0.15. Thus, at this setting most significant level of waveform animation is achieved.

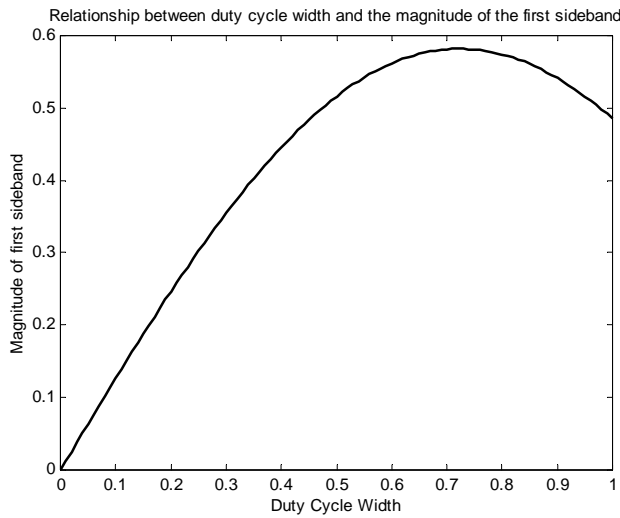


Figure 5. Relationship between the duty cycle width and first sideband magnitude computed using (20).

5. ANIMATOR USING A DELAY LINE FILTER

The multiple detuned oscillator effect can also be created by employing a group of delay-line based pitch shifters and a single waveform input [48]. The principle can be seen as an extension of the use of inverse comb filters with time-varying delays. By combining the output of such delay lines with the original signal, we will be able to model the multiple detuned oscillator effect for arbitrary inputs.

The pitch shifter operation is based on a periodic linear change in delay time. The amount of pitch transposition is proportional to the rate of delay change [49]. By modulating a delay line with a signal whose derivative is constant and non-zero, the pitch of the input signal can be shifted. We can define this process for a single up and down transposition pair by the following expressions, where τ is the delay line length, s is the frequency scaling factor (transposition ratio) and $x(t)$ is the input signal:

$$S_{wa,dl}(t) = w(\gamma(t))x(t - D(\gamma(t), \tau)) + w(\gamma(t) + \frac{1}{2})x(t - D(\gamma(t) + \frac{1}{2}, \tau)) \quad (24)$$

where the delay modulation signal $\gamma(t)$ is defined as

$$\gamma(t) = (\frac{s-1}{\tau})t - \left\lfloor (\frac{s-1}{\tau})t \right\rfloor \quad (25)$$

The windowing and delay functions in (24), $w(x)$ and $D(x)$ are expressed by

$$w(x) = 0.5 + 0.5\cos(2\pi x) \quad (26)$$

and

$$D(x, d) = xd + \left\lfloor \frac{xd}{d} \right\rfloor d \quad (27)$$

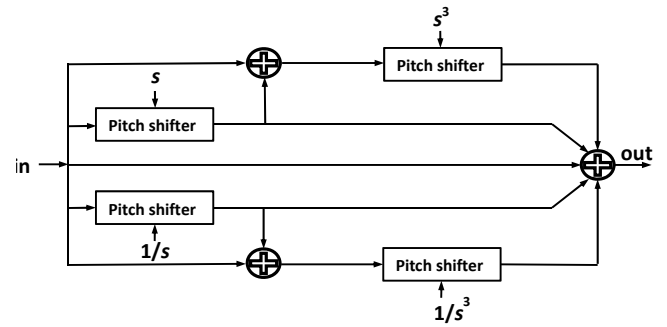


Figure 6. The pitch-shifter based detuned oscillator effect where s is the transposition factor $1 + \delta f_0/f_0$.

The windowing is necessary to hide the discontinuities of signal as the delay jumps from 0 to τ . The use of two delay lines is designed to allow crossfading between them, which creates a continuous pitch-shifted signal.

To create a mix of seven signals with slight tuning differences, we can use four pitch shifters arranged as in the block diagram in Fig. 6. The transposition factor s should then be set to $1 + \delta f_0/f_0$, providing a constant-interval spacing between each pitch-shifted copy of the original signal.

An example of the waveform output and the magnitude spectrum is given in Fig. 7. The upper panel shows the waveform over a 9 second period. The envelope of the waveform shows periodic peaks and troughs due to the beating that is occurring between the detuned harmonics. The two plots in the lower panel show the cluster of components around the region of the first harmonic and the second harmonic of the input. As expected the bandwidth around the second harmonic is proportionally wider than that of the first.

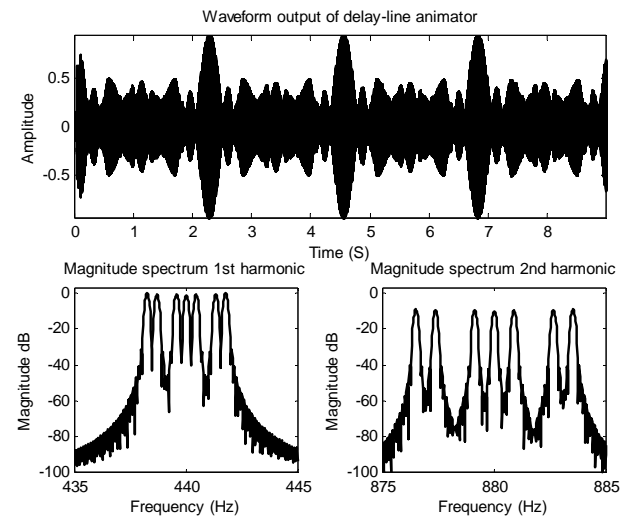


Figure 7. The pitch-shifter based detuned oscillator effect, where s is the transposition factor $1 + \delta f_0/f_0$. The upper panel shows the waveform output and the lower panels shows the magnitude spectrum in the region around the first and second harmonics of the input waveform respectively.

6. CONCLUSION

This paper has investigated the digital implementation of a Waveform Animator oscillator effect. It has first presented a mathematical analysis that has resulted in expressions for the frequency spectra of this effect, looking in detail at the significance of the modulation components. Secondly, it examined by simulation the relationship between the duty cycle and the degree of animation. Lastly, a delay line based algorithm was then discussed as means to obtain a general model of this effect. Furthermore, if the input to the delay-line model is bandlimited then the output will also be so. Such a model could be incorporated within any synthesis toolkit. It is intended that this work will offer sound designers more insight into alternative approaches for synthesizing ‘Supersaw’ timbres and also raise their awareness as to the role that frequency modulation plays within these sounds.

7. REFERENCES

- [1] J. Pakarinen, V. Välimäki, F. Fontana, V. Lazzarini, and J. Abel, “Recent advances in real-time musical effects, synthesis, and virtual analog models,” *EURASIP Journal on Advances in Signal Processing*, vol. 2011, 2011.
- [2] J. Pakarinen and D. T. Yeh, “A review of digital techniques for modeling vacuum-tube guitar amplifiers,” *Computer Music Journal*, 33(2), Summer 2009, pp. 85-100.
- [3] J. Pakarinen and M. Karjalainen, “Enhanced wave digital triode model for real-time tube amplifier emulation,” *IEEE Trans. Audio, Speech, and Language Processing: Special Issue on Virtual Analog Modeling*, vol. 18, no. 4, pp. 738-746, May 2010.
- [4] D. Yeh. and J. O. Smith, “Simulating guitar distortion circuits using wave digital and nonlinear state-space formulations,” in *Proc. 11th Int. Conf. Digital Audio Effects (DAFx-08)*, Espoo, Finland, Sept. 2008.
- [5] D. Yeh, *Digital Implementation of Musical Distortion Circuits by Analysis and Simulation*. Ph.D. thesis, Stanford University, Stanford, CA, USA, June 2009. <https://ccrma.stanford.edu/~dtyeh/papers/pubs.htm>
- [6] V. Välimäki, J. Parker, and J. S. Abel, “Parametric spring reverberation effect,” *J. Audio Eng. Soc.*, vol. 58, no. 7/8, pp. 547–562, July/August 2010.
- [7] V. Välimäki and A. Huovilainen, “Antialiasing oscillators in subtractive synthesis,” *IEEE Signal Processing Magazine*, vol. 24, no. 2, pp. 116-115, March 2007.
- [8] V. Lazzarini and J. Timoney, “New perspectives on distortion synthesis for virtual analogue oscillators,” *Computer Music Journal*, vol. 34, no. 1, pp. 28-40, Mar. 2010.
- [9] J. Kleimola, V. Lazzarini, J. Timoney, and V. Välimäki, “Phaseshaping oscillator algorithms for musical sound synthesis,” in *Proc. 7th Sound and Music Computing Conference*, Barcelona, Spain, July 2010, pp. 94–101.
- [10] J. Pekonen, V. Lazzarini, J. Timoney, J. Kleimola, and V. Välimäki, “Discrete-time modelling of the Moog sawtooth oscillator waveform,” *EURASIP Journal on Advances in Signal Processing*, 2011.
- [11] A. Huovilainen, *Design of a Scalable Polyphony-MIDI Synthesizer*. M.S. thesis, Aalto University, Espoo, Finland, May 2010, <http://lib.tkk.fi/Dipl/2010/urn100219.pdf>.
- [12] T. Helie, “Volterra series and state transformation for real-time simulations of audio circuits including saturations: application to the Moog ladder filter,” *IEEE Trans. Audio, Speech and Language Processing*, vol. 18, no. 4, pp. 747-759, May 2010.
- [13] F. Fontana and M. Civolani, “Modeling the EMS VCS3 voltage-controlled filter as a nonlinear filter network,” *IEEE Trans. Audio, Speech and Language Processing*, vol. 18, no. 4, pp. 760-772, May 2010.
- [14] G. De Sanctis and A. Sarti, “Virtual analog modeling in the wave digital domain,” *IEEE Trans. Audio, Speech and Language Processing*, vol. 18, no. 4, pp. 715-727, May 2010.
- [15] J. Lane, D. Hoory, E. Martinez, and P. Wang, “Modeling analog synthesis with DSPs,” *Computer Music Journal*, vol. 21(4), 1997, pp. 23–41.
- [16] D. Ambrits and B. Bank, “Improved polynomial transition regions algorithm for alias-suppressed signal synthesis,” in *Proc. Sound and Music Computing Conf. (SMC 2013)*, Stockholm, Sweden, pp. 561-568, Aug. 2013.
- [17] S. Tassart, “Band-limited impulse train generation using sampled infinite impulse responses of analog filters,” *IEEE Trans. Audio, Speech, and Language Processing*, vol. 21, no. 3, pp. 488-497, Mar. 2013.
- [18] J. Pekonen and M. Holters, “Nonlinear-phase basis functions in quasi-bandlimited oscillator algorithms,” in *Proc. 15th Intl. Conf. Digital Audio Effects (DAFx-12)*, York, UK, pp. 261-268, 2012.
- [19] J. Kleimola and V. Välimäki, “Reducing aliasing from synthetic audio signals using polynomial transition regions,” *IEEE Signal Processing Letters*, vol. 19, no. 2, pp. 67-70, Feb. 2012.
- [20] R. Snoman, *The Dance Music Manual*. Focal press, Elsevier, Oxford, UK, 2004.
- [21] G. Winham and K. Steiglitz, “Input generators for digital sound synthesis,” *J. Acoust. Soc. Amer.*, vol. 47, part 2, pp. 665-666, Feb. 1970.
- [22] T. Stilson and J. O. Smith, “Alias-free digital synthesis of classic analog waveforms,” in *Proc. Int. Computer Music Conf.*, Hong Kong, pp. 332-335, 1996.
- [23] T. Stilson, *Efficiently-Variable Non-Oversampled Algorithms in Virtual-Analog Music Synthesis - A Root-Locus Perspective*. Ph.D. thesis, Stanford University, Stanford, CA, USA, June 2006. <http://ccrma.stanford.edu/~stilti/papers/Welcome.html>.
- [24] J. Nam, V. Välimäki, J. S. Abel, and J. O. Smith, “Alias-free virtual analog oscillators using a feedback delay loop,” in *Proc. 12th Intl. Conf. Digital Audio Effects (DAFx-09)*, Como, Italy, September 1-4, 2009.
- [25] J. Nam, V. Välimäki, J. S. Abel, and J. O. Smith, “Efficient antialiasing oscillator algorithms using low-order fractional delay filters,” *IEEE Trans. Audio, Speech and Language Processing*, vol. 18, no. 4, pp. 773–785, May 2010.

- [26] V. Välimäki, "Discrete-time synthesis of the sawtooth waveform with reduced aliasing," *IEEE Signal Processing Letters*, vol. 12, no. 3, pp. 214-217, March 2005.
- [27] V. Välimäki, J. Nam, J. O. Smith, and J. S. Abel, "Alias-suppressed oscillators based on differentiated polynomial waveforms," *IEEE Transactions on Audio, Speech and Language Processing*, vol. 18, no. 4, pp. 786-798, May 2010.
- [28] V. Välimäki and A. Huovilainen, "Oscillator and filter algorithms for virtual analog synthesis," *Computer Music Journal*, vol. 30, no. 2, pp. 19-31, 2006
- [29] J. Timoney, V. Lazzarini, and T. Lysaght, "A modified FM synthesis approach to bandlimited signal generation," in *Proc. 11th Intl. Conf. Digital Audio Effects (DAFx-08)*, Espoo, Finland, pp. 27-33, Sept. 1-4, 2008.
- [30] V. Välimäki, J. Pekonen and J. Nam, "Perceptually informed synthesis of bandlimited classical waveforms using integrated polynomial interpolation," *J. Acoust. Soc. Amer.*, vol. 131, no. 1, pt. 2, pp. 974-986, Jan. 2012.
- [31] E. Brandt, "Hard sync without aliasing," in *Proc. Int. Comp. Music Conf.*, Havana, Cuba, Sept. 17-22, 2001.
- [32] J. Timoney, V. Lazzarini, M. Hodgkinson, J. Kleimola, J. Pekonen, and V. Välimäki, "Virtual analog oscillator hard sync: Fourier series and an efficient implementation," in *Proc. 15th Intl. Conf. Digital Audio Effects (DAFx-12)*, York, UK, September 17-21, 2012.
- [33] D. Lowenfels, "Virtual analog synthesis with a time-varying comb filter," *AES Convention 115*, New York, NY, USA, Oct. 10-13, 2003.
- [34] J. Timoney, and V. Lazzarini, "Exponential frequency modulation bandwidth criterion for virtual analog applications," in *Proc. 14th Intl. Conf. Digital Audio Effects (DAFx-11)*, Paris, France, Sept. 19-23, 2011.
- [35] B. Hutchins, "Analog circuits for sound animation," *J. Audio Eng. Soc.*, vol. 29, no. 11, pp 814-820, Nov. 1981.
- [36] M. Russ, *Sound Synthesis and Sampling*. Focal press, Elsevier, Oxford, UK, 2009.
- [37] Moog Music Inc., *Minimoog Voyager Old School user's manual*, 2008. [HTTP://WWW.BIGBRIAR.COM/MANUALS/OLD_SCHOOL_MANUAL_1_0.PDF](http://www.bigbriar.com/Manuals/OLD_SCHOOL_MANUAL_1_0.PDF).
- [38] Roland Corporation, *JP-8000 Owner's Manual*. 1996. [Online]. <http://www.rolandus.com>.
- [39] Roland Corporation, *Jupiter-8 Owner's manual*, 1983. [FTP://FTP.ROLAND.CO.UK/PRODUCTSUPPORT/JP-8/01_JP-8_OM.PDF](ftp://ftp.roland.co.uk/PRODUCTSUPPORT/JP-8/01_JP-8_OM.PDF)
- [40] Sequential Circuits, *Prophet 5 Owner's manual*, 1977 [WWW.SUONOELETRONICO.COM/DOWNLOADS/PROPHET5MANUAL.PDF](http://www.suonoelettronico.com/downloads/PROPHET5MANUAL.PDF)
- [41] Access Music Electronics GMBH, Access TI Quick Start manual, [HTTP://WWW.ACCESSMUSIC.DE/PAGE/RENDER/LANG/EN/P/15/DO/SUPPORT_CONTACT_AND_RESOURCES.HTML](http://www.accessmusic.de/page/render/lang/en/p/15/do/support_contact_and_resources.html).
- [42] J. C. Risset, "Examples of the musical use of digital audio effects," *J. New Music Research*, vol. 31, no. 2, pp. 93-97, June 2002.
- [43] D. Trueman, P. Cook, S. Smallwood and G. Wang, "PLOrK: The Princeton Laptop Orchestra, Year 1," in *Proc. Int. Comp. Music Conf.*, New Orleans, LA, USA, Nov. 6-11, 2006.
- [44] W. Hartmann, *Signals, Sound and Sensation*, Springer, USA, 2005.
- [45] R. Guinee, "A novel Fourier series simulation tool for pulsewidth modulation (PWM) in pulsed power systems," in *Proc. IEEE 22nd Symp. Fusion Eng.*, Albuquerque, NM, USA, 17-21 June 2007, pp. 1-4.
- [46] M. LeBrun, "A Derivation of the Spectrum of FM with a Complex Modulating Wave," *Computer Music Journal*, vol. 1, no. 4, pp. 51-52, Winter 1977.
- [47] G. Watson, *A Treatise on the Theory of Bessel Functions*. Cambridge university press, Cambridge, UK, 1995.
- [48] K. Bogdanowicz and R. Belcher, "Using multiple processors for real-time audio effects," in *Proc. Audio Eng. Soc. 7th Int. Conf.*, May 1989, pp. 337-342.
- [49] S. Disch and U. Zolzer, "Modulation and delay line based digital audio effects," in *Proc. 2nd Int. Conf. Digital Audio Effects (DAFx-99)*, Trondheim, Norway, pp. 5-8, Sept. 9-11, 1999.